

# Avalanche Photodiodes

Design and Applications

S.E. Nickols, CTO , Diablo Mountain Research, LLC

## I. Avalanche Photodiodes and Their Applications

Avalanche Photodiodes (APDs) are semiconductor photodetectors designed to detect extremely low-intensity optical signals with fast response times resulting from the avalanche multiplication of carriers created via light absorption.

APDs have similar structures to P-I-N photodiodes, except their design features a moderately doped region, allowing carrier multiplication at a specific bias. Their active areas vary from tens of  $\mu\text{m}$  to over 10 millimeters in diameter.

APDs can be considered an alternative to photomultiplier tubes. They operate at a lower bias, in a smaller configuration, with very high reliability and the ability to withstand various environmental conditions. However, they exhibit a lower dynamic range in comparison.

Avalanche photodiodes are used in a variety of applications in scientific research and industries, including:

- Semiconductor Fabrication Equipment
- LiDAR and Rangefinders
- Laser Scanners
- Medical Imaging
- Molecular Imaging
- High Energy Physics
- Analytical Instruments
- Military Applications
- Optical Communication

## II. Avalanche Multiplication Basics

With its unique ability to enhance the photodiode signal, avalanche multiplication has been known since the late 1950s.

Similar to a simple P-I-N photodiode, a typical APD is manufactured from a slab of Silicon, uniformly doped with a p-type dopant and forming the Anode and the Cathode on the slab sides.

Applying a reverse bias across the Silicon slab creates an electric field, and non-equilibrium carriers created through light absorption accelerate in this field. The higher the electric field, the higher the energy and the momentum of each carrier. Drifting carriers collide with the dopant atoms, and if the carrier energy is high enough, it ionizes the dopant atom creating additional free carriers through impact ionization. The avalanche multiplication occurs when the electric field across the semiconductor bulk reaches the critical value,  $E_{cr}$ , as schematically shown in Figure 1. The higher the electric field, the larger the avalanche multiplication.

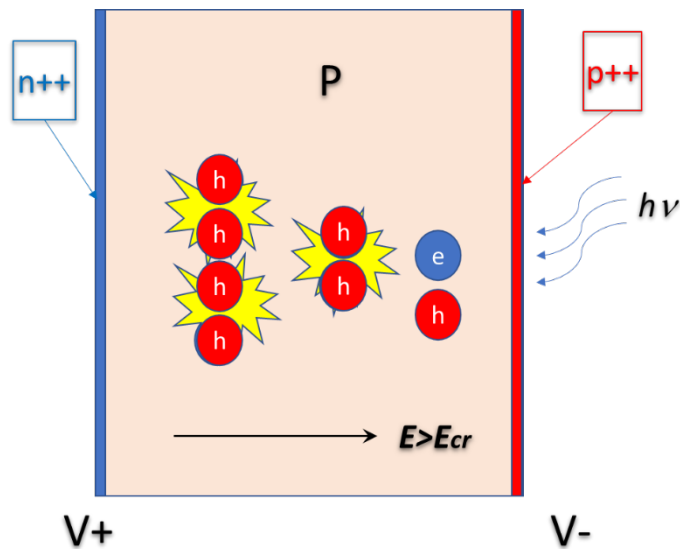


Figure 1. Avalanche Multiplication. Only the additional free holes created through avalanche multiplication are shown for simplicity

The critical electric field and the impact ionization coefficients for electrons and holes are unique for different semiconductor materials.

The ionization coefficient - (*alpha*) for electrons and (*beta*) for holes - depends on the electric field strength  $E$  and the ratio between the two controls the avalanche multiplication features in different semiconductors:

$$k(E) = \frac{b(E)}{a(E)} \quad (1)$$

Electrons, holes, or both can start the avalanche depending on the semiconductor material.

### III. APDs: Key Performance Parameters

- Avalanche Gain (or Multiplication Factor)
- Noise
- Operating Bias
- Temperature Dependence
- Response Time and Gain Bandwidth

An optimal APD structure can be designed based on the desired performance. For any APD structure, the avalanche gain and noise depend on several parameters, which are theoretically challenging to analyze. The analysis can be simplified if reasonable assumptions are made. One of the crucial assumptions is that all non-equilibrium carriers are equal and participate in avalanche multiplication equally.

### a. APD Gain

Suppose one assumes position-independent and equal ionization coefficients for both electrons and holes. In that case, the avalanche gain over the depleted thickness ( $W$ ) of a semiconductor for carriers injected at its edge can be approximated by the following formula:

$$M = (1 - \alpha(E)W)^{-1} \quad (2)$$

If the ionization coefficients are not equal, however, the avalanche gain over the depleted thickness is more complex:

$$M = \frac{(1-\beta/\alpha)\exp[-\alpha W(1-\beta/\alpha)]}{1-\beta/\alpha\exp[-\alpha W(1-\beta/\alpha)]} \quad (3)$$

Measuring the avalanche gain by experiment is straightforward and is explained in the future chapters.

### b. APD Noise

Using Poisson statistics for the shot noise - the main contributor to the noise current for any  $P$ - $I$ - $N$  photodiode and  $APD$  - and assuming that the gain is the same for any event at selected bias, the shot noise current density of the  $APD$  is:

$$i_n = \sqrt{2q(I_{light} + I_{dark-bulk})M^2 + 2qI_{dark-surface}} \quad (4)$$

$$\frac{S}{N} = \frac{I_{signal}}{i_n} = \frac{MxI_{primary}}{Mxi_{n-primary}} = \frac{I_{primary}}{i_{n-primary}} \quad (5)$$

When compared to a P-I-N photodiode, assuming equal gain for all carriers, an ideal APD provides the output signal with  $M$ -times higher amplitude than a P-I-N photodiode, with an almost equal signal-to-noise ratio of the same size P-I-N photodiode.

The assumption that "equal gain ( $M$ ) for each carrier is not correct" was first shown by McIntyre [1] and later developed by Campbell's group [2], confirming that the probability of creating an avalanche is widely distributed. Figure 2 shows the probability for ten initially identical electrons to create an avalanche for different values of the avalanche gain and two different  $k$ -values. The probability is well below unity for any gain. This creates substantial additional noise in the APD, which may cause the device to be impractical.

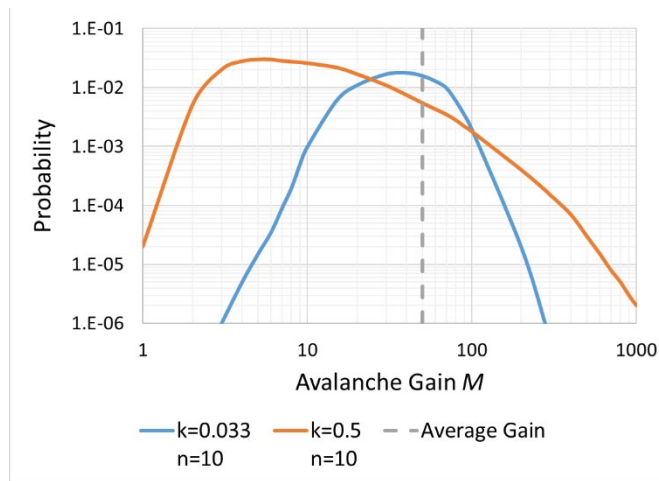


Figure 2. Probability for  $n$  injected electrons/holes to result in  $M \cdot n$  avalanche electrons/holes

By taking the effects of the gain non-uniformity into account, the equation for the noise current density must be re-written for average values:

$$\langle i_n \rangle = \sqrt{2q(I_{light} + I_{dark-bulk})\langle M^2 \rangle + 2qI_{dark-surface}} \quad (6)$$

McIntyre introduced the factor  $F(M)$ , which describes an increase in the noise value due to the gain of non-uniformity. By substituting  $\langle M^2 \rangle$  with its theoretical value  $\langle M^2 \rangle = M^2 F(M)$  the correct expression for the average noise current is obtained by:

$$\langle i_n \rangle = \sqrt{2q(I_{light} + I_{dark-bulk})M^2F(M) + 2qI_{dark-surface}} \quad (7)$$

Where  $M$  is the average gain, and  $F$  is the excess noise factor introduced by McIntyre. To improve the APD performance, ideally, it is crucial to minimize the excess noise factor ( $F$ ) to a value of 1. This is one of the primary requirements for high-performance APDs.

### c. APD Noise: Factors Influencing $F(M)$

The wide distribution of carriers over their efficiency to create an avalanche produces large excess noise, leading to a large value of the excess noise factor ( $F$ -factor).

The distribution width of the gain probability for carriers must be narrower to reduce the  $F$ -factor value. This can be achieved by using the following approaches:

- Select a structure in which only one carrier type participates in multiplication. This creates a 2x narrower distribution and hence, a smaller excess noise factor.
- A thinner multiplication region may create a narrower gain distribution and thus a lower  $F$ -factor value.
- Higher doping uniformity in the multiplication region also narrows the distribution and reduces the excess noise factor value.
- Lowering operating bias reduces the  $F$ -factor value.

Some of these approaches are discussed further in detail in the following chapters.

## IV. Basic APD Structures

One of the primary requirements for any basic APD structure is supporting a high electric field ( $E > E_{cr}$ ) to achieve the avalanche multiplication.

### a. Reach-Through APD Structures

The so-called Reach-Through Structures operate under a complete depletion of the entire thickness of the semiconductor's active region and applying a heavily doped Anode and Cathode to support the critical electric field.

In this scenario, a lightly doped p-type Silicon slab is fabricated with a heavily doped Anode on the bottom and a Cathode on the top (Figure 3). Theoretically, when a reverse bias is applied, the electric field reaches its critical value at a specific voltage. As shown in Figure 3, the structure can support a high electric field because the guard ring and edge channel stoppers help avoid early breakdown and support a high electric field across the whole thickness of the die.

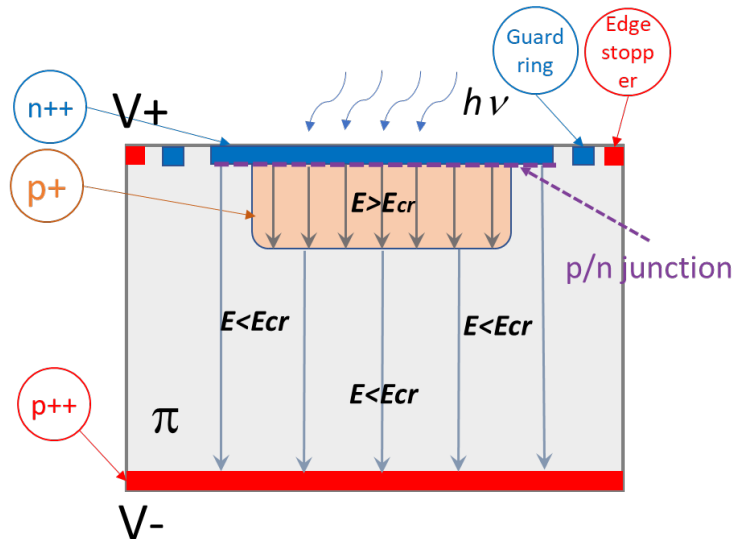


Figure 3. Reach-Through APD Structures

Moreover, to improve the uniformity of the avalanche multiplication, creating a dedicated avalanche multiplication layer, sometimes referred to as a "p-well," with a moderate dopant p+ concentration is advantageous.

By applying a reverse bias, the electric field reaches its critical value only within a thin layer p+ (p-well), and avalanche multiplication conditions are satisfied within this layer only. In this case, the edge dark current is not subject to avalanche multiplication, and this structure can support the high bias necessary to reach high avalanche gain.

### b. Bevel-Edge Terminated APD Structures

In Bevel-Edge Terminated APD Structures (see Figure 4), the avalanche region (p+) is a whole epi layer. The die is modified by beveling edges to support a high electric field. This allows redistributing the electric field lines, making their density at the die's edges much lower than in the middle.

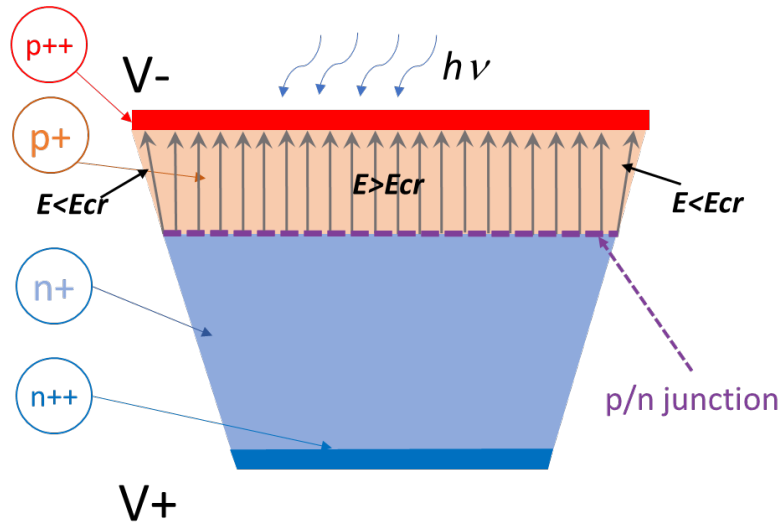


Figure 4. Bevel Edge terminated APD structures

By applying a reverse bias, the electric field reaches its critical value in the middle portion of the epi layer but not at the edges. As a result, the avalanche multiplication progresses uniformly everywhere except the edges. The dark current generated at the edges of the die does not take part in avalanche multiplication.

## V. Methods to Improve Excess Noise in APD

There are a few approaches that can improve the excess noise of APDs:

- Design structures that allow only one type of carrier to participate in multiplication. This may employ the so-called Separate Absorption and Charge-Multiplication (SACM) regions used in compound semiconductors and Ge-Si APDs.
- Creating a narrower, more uniform multiplication region is achieved by using thin epi layers and buried multiplication layers in Si, Ge, and compound semiconductors
- Adding certain structural elements to improve gain uniformity further

### a. Separate Absorption and Charge Multiplication Regions

Figure 5 exhibits the schematic of an InGaAs APD structure with the p-type absorption region close to the light entry side. All light quanta are absorbed in this region, and the generated non-equilibrium electrons are swept by the electric field toward the multiplication region at the bottom of the structure, creating an avalanche. The non-equilibrium holes drift toward the Anode on the top and do not participate in avalanche multiplication.

Typical values for the excess noise factor for InGaAs APDs is  $\sim 10$ ; however, some recently reported structures report the F-factor value of around 3 with the avalanche gain of  $\sim 40$ .

### InGaAs-based APDs (e-injection):

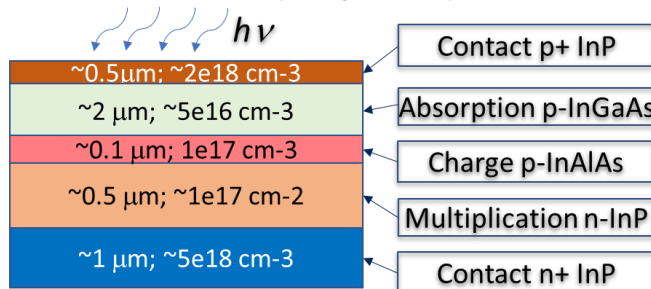


Figure 5. InGaAs-based APDs with Separate Absorption and Charge Multiplication Regions

Figure 6 shows a Ge-Si APD structure where the Germanium absorption layer is close to the light entry side. All light quanta are absorbed in the Germanium absorption layer by illuminating the structure with infrared light. The generated non-equilibrium electrons are swept by the electric field toward the Silicon multiplication region at the bottom of the structure, creating the avalanche. Silicon is characterized by better ionization coefficients for electrons than germanium, which makes Silicon a preferred multiplication layer. The non-equilibrium holes drift toward the Anode on the top and do not participate in avalanche multiplication.

Typical values for the excess noise factor achieved for Ge-Si APDs is  $\sim 3$  with the avalanche gain of  $\sim 30$ .

### Ge-Si APDS (e-injection):

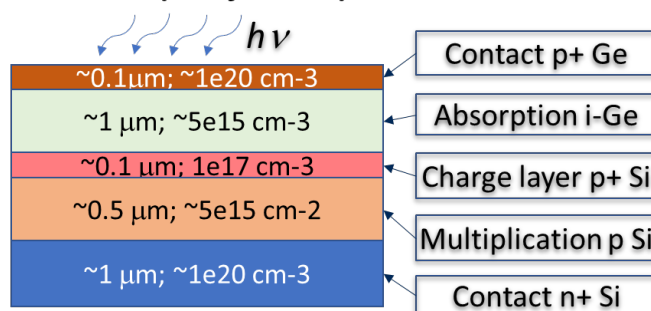


Figure 6. Ge-Si APDs with Separate Absorption and Charge Multiplication regions

## b. Thin Buried Multiplication Layer

Another method to improve  $F$ -factor is to create a narrower and more uniform multiplication region, which produces narrower gain distribution and hence, lowers  $F$ -factor values. This is attained by fabricating thin epi layers and deep implanted (or buried) multiplication layers in Si, Ge, and compound semiconductors. (Figure 7)

A buried multiplication layer p+ can be created underneath the front-side Cathode with small spacing for Silicon devices. It excludes specific surface dark currents from multiplication and creates a more uniform electric field within the avalanche layer.

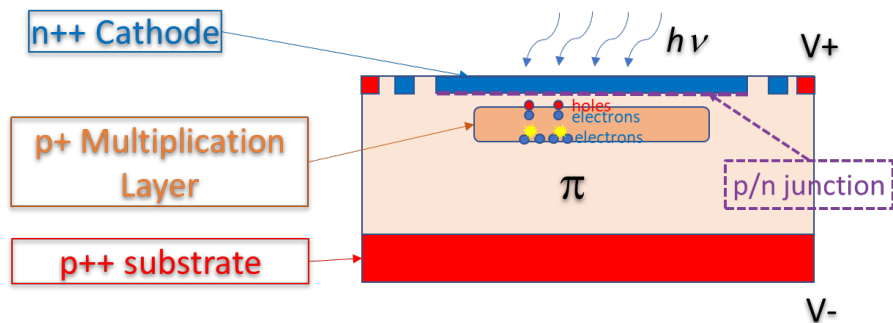


Figure 7. Example of Si APD with buried multiplication layer

By applying a reverse bias and illuminating the diode, non-equilibrium electrons participate in the avalanche process within the multiplication layer. Typical  $F$ -factor values vary from 2 to 10 at the gain value of  $\sim 100$  for Silicon at 23 °C for this structure.

### c. Bevel-Edge Terminated Structures

Adding structural elements with a bevel-edge terminated large active area silicon APD is another method to reduce the  $F$ -factor.

Figure 8 shows a large area Silicon APD with a top p++ contact. The p+ multiplication epi layer is fully depleted but not necessarily the N-type substrate. The p++ contact ring on the top provides the necessary support for beveling and serves as a top contact.

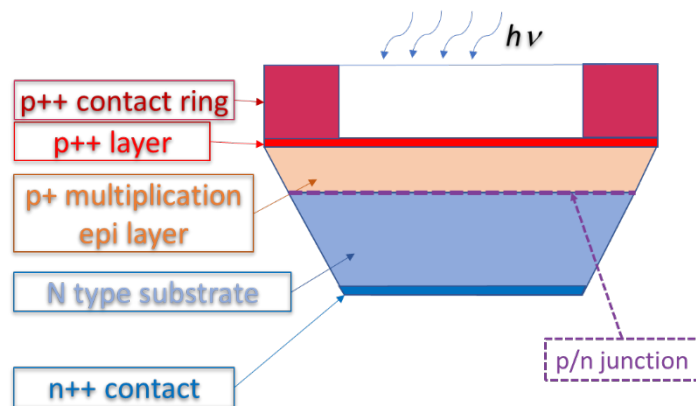


Figure 8. Example of Si Large Area APD (LAAPD) with beveled edges

This structure operates at a reverse bias between 1500V and 2100V with the gain of more than 300 at  $T=23^{\circ}\text{C}$  and *greater* than 400 at zero Celsius. It allows the production of APDs with the industry's lowest  $F$ -factor values. The spectral sensitivity range extends from vacuum UV to 1000 nm. The excess noise factor is typically less than 1.3 for the gain of 300 at  $T=23^{\circ}\text{C}$  and the noise current spectral density per  $\text{mm}^2$  active area is below  $2.0 \times 10^{-14} \frac{\text{A}}{\sqrt{\text{Hz}}}$  at  $T=23^{\circ}\text{C}$ . This is more than ten (10) times better than any other APD.

## VI. Evaluation of APD Parameters

Evaluation of Avalanche Gain, quantum efficiency (QE), capacitance, and other critical performance parameters of APDs are discussed in this section.

### a. Avalanche GAIN

A front-illuminated Silicon APD with a buried avalanche layer structure and the dark and light current-voltage characteristics are shown in Figures 9 and 10, respectively.

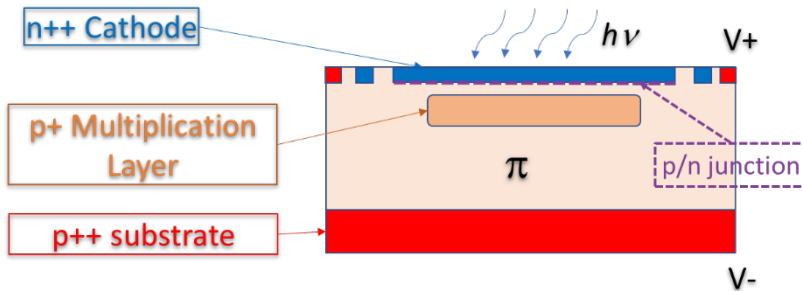
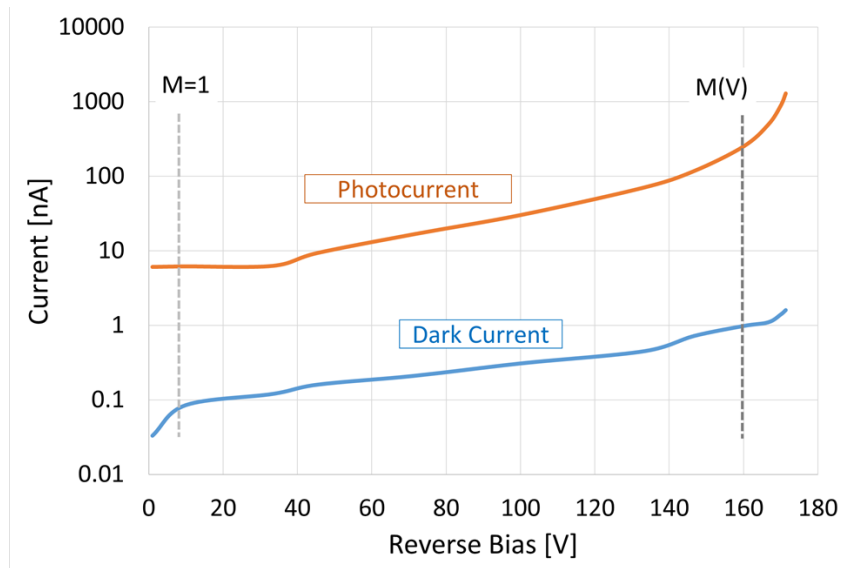


Figure 9. APD structure with buried multiplication layer



*Figure 10. Typical dark current and photocurrent for APD structure with buried multiplication layer*

The gain at the bias  $V$ , is the difference between the photocurrent and dark current at the operating bias  $V$  divided by the difference between the photocurrent and dark current at unity gain:

$$M(V) = \frac{I_{photo}(M(V)) - I_{dark}(M(V))}{I_{photo}(M=1) - I_{dark}(M=1)} \quad (8)$$

## b. Quantum Efficiency and Gain

Figure 11 shows the same structure's quantum efficiency (QE) measured at unity gain. QE is usually determined at the operating bias producing unity Gain ( $M=1$ ).

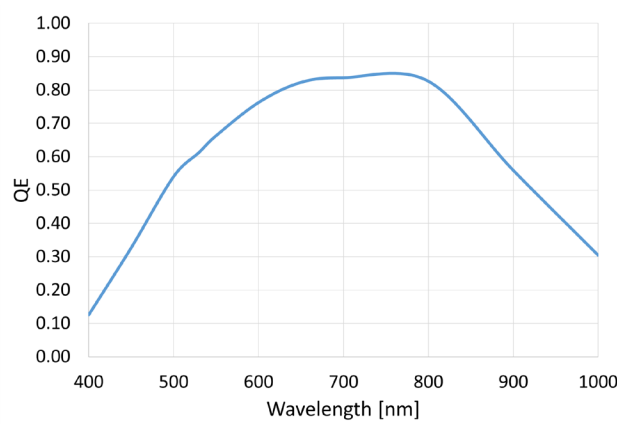


Figure 11. Typical Quantum Efficiency of APD-800 at  $M=1$ .

Assuming the structure is optimized for the wavelength range of around 800 nm, the gain dependence on the reverse bias at 800 nm is obtained using the method described previously (see Figure 12). The gain remains at unity up to approximately 40V, then rises. At around 45V, the dependence starts to level-down (shown with a green arrow in Figure 12), indicating completion of the multiplication layer depletion.

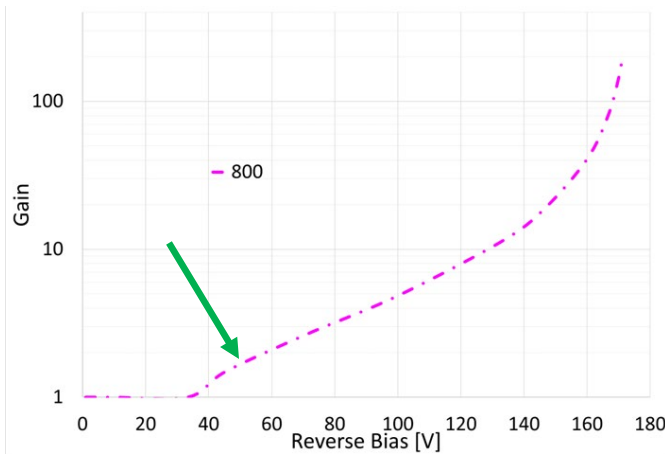


Figure 12. Typical gain for APD-800 at 800nm

For APD-800 of the structure shown in Figure 9, the gain behavior at other wavelengths differs from 800 nm. At longer wavelengths, the gain is high, but the quantum efficiency is very low (Figure 13), and the overall sensitivity is low.

The gain is very low at short wavelengths because the absorption depth does not reach the buried multiplication layer. Only the holes and a small portion of electrons created by light absorption contribute to the avalanche process. Since the impact ionization rate for holes in Silicon is much lower than for electrons, the holes do not contribute significantly to the avalanche current.

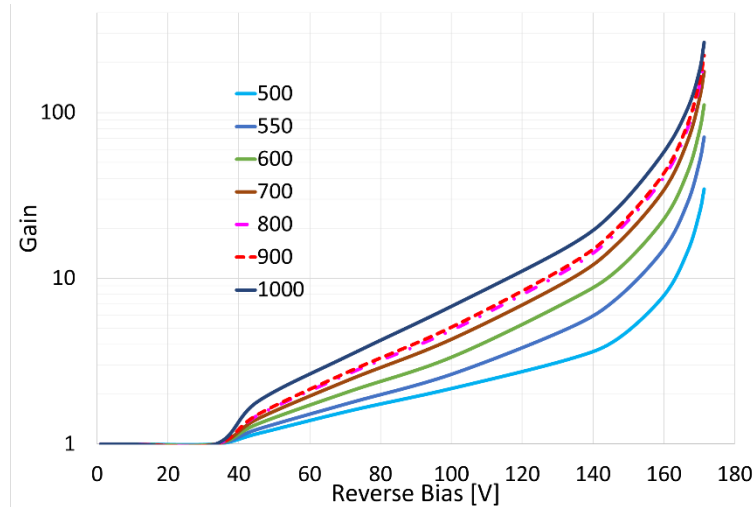


Figure 13. Typical gain of APDE-800 for various wavelengths

### c. Capacitance

The APD capacitance dependence on the reverse bias reveals features that can be correlated to certain features of the avalanche gain dependence on voltage.

Figure 14 exhibits a slow decrease in the capacitance value with reverse bias up to  $\sim 45\text{V}$  due to the depletion edge propagating through the p+ multiplication layer. At around 45V, the entire thickness of the multiplication layer is depleted, signaled by the beginning of a sharp drop in the capacitance value and a kink shown with an arrow in the main plot of Figure 12. Further increase of the applied bias leads to a fast propagation of a depletion edge through the p- layer. The capacitance saturation is evidenced at  $\sim 60\text{V}$  bias when the reach-through conditions are reached. Raising the bias beyond  $\sim 60\text{V}$  causes the electric field within the avalanche region to increase dramatically, creating a steady increase in avalanche gain at 800 nm.

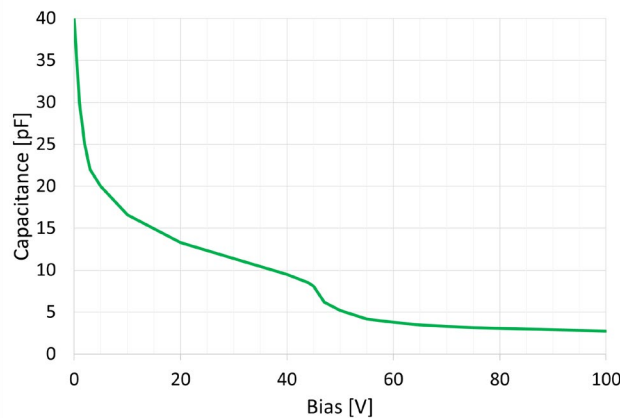


Figure 14. Typical capacitance for APD-800

### d. Gain and QE for a Back-Illuminated Si APD

A backside-illuminated structure improves the UV sensitivity of Silicon APDs, as shown in Figures 15 and 16.

The n+ Cathode is placed at the bottom of the absorption p region while the p+ Anode is on the top next to the p/n junction. The interconnect layer enables all contacts to be brought to the top surface of the structure.

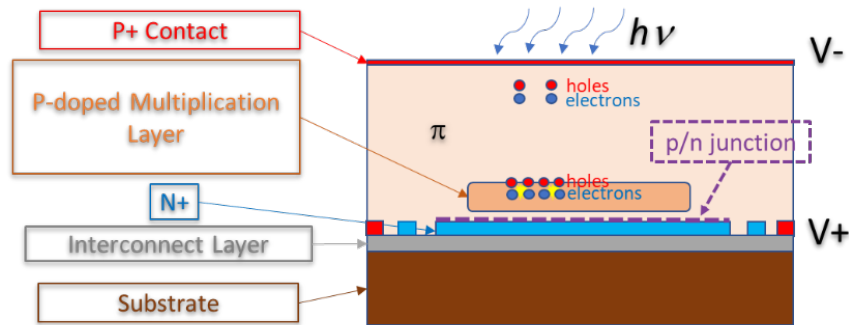


Figure 15. Schematics of a typical backside-illuminated APD

Under illumination, the UV light is completely absorbed close to the top surface, and non-equilibrium carriers start to drift toward respective electrodes. When they reach the multiplication layer, electrons have enough energy to start impact ionization, creating the avalanche. The back-illuminated structure's quantum efficiency in the short-wavelength spectral range is significantly improved (Figure 16).

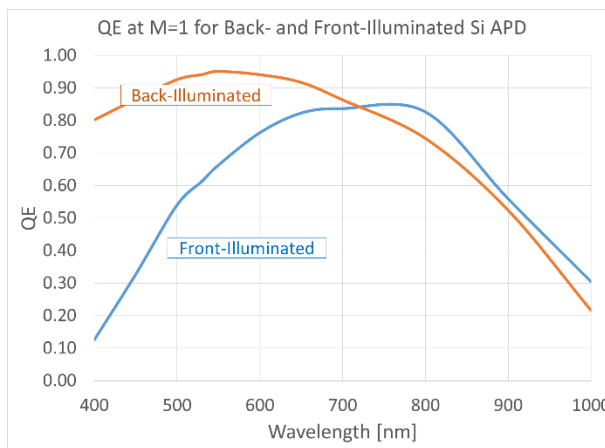


Figure 16. Quantum efficiency of a sample back-illuminated APD

The gain for the short-wavelength range becomes higher, reaching the values characteristic for the front-illuminated structure in the long-wavelength spectral range (Figure 17).

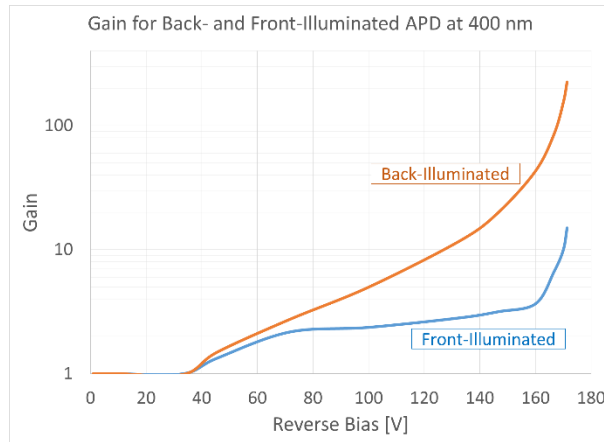


Figure 17. Gain of sample back-illuminated and front-illuminated APDs at 400nm

### e. Excess Noise Factor

One of the most challenging parameters to estimate is the excess noise factor of APDs. Each APD design requires a unique approach. In some cases, determining the *F*-factor value is more an art than a science.

The Noise Spectral Density for an APD is determined primarily by the shot noise obeying the Poisson distribution.

In practice, the dark conditions are used to estimate the excess noise factor :

$$\langle i_n \rangle = \sqrt{2q[I_{dark-bulk}(V)]M(V)^2F(M(V)) + 2qI_{dark-surface}} \quad (9)$$

Figure 18 exhibits the required parameters for estimating the  $F$ -factor. They include the light and dark currents at both the unity gain and gain of interest. Only the bulk portion of the dark current is multiplied in the avalanche region, and the surface dark current is not multiplied and does not affect the gain. In some instances, the surface dark current is independent of the applied bias, making the  $F$ -factor estimate simple.

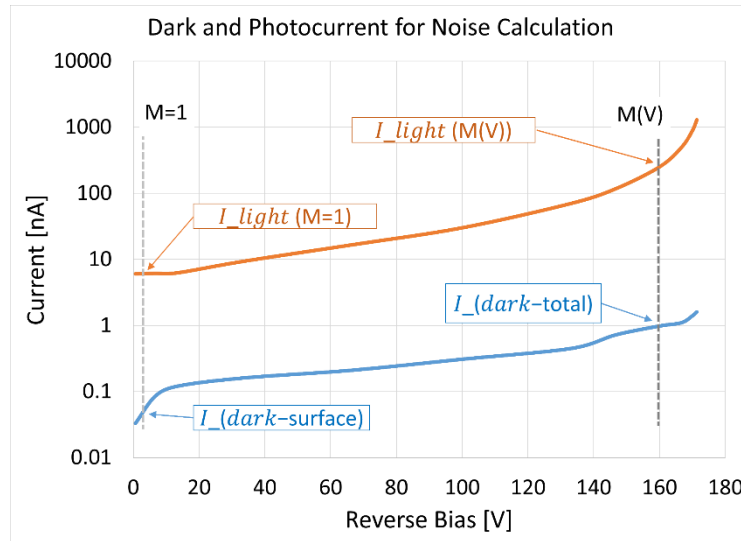


Figure 18. Definitions of the dark and photocurrent for noise calculation

To estimate the F-factor:

1. The dark noise current spectral density  $\langle i_n \rangle$  is measured, at the bias of interest, by a spectrum analyzer or lock-in amplifier.
2. Estimate the dark bulk current from the data shown in Figure 18 by assuming that the dark current is primarily due to the surface current at a low bias value, and the surface dark current does not change with bias.
3. Calculate the gain at each bias of interest by using the light and dark current values from Figure 18,

$$M(V) = \frac{I_{light}(M(V)) - I_{dark-total}(M(V))}{I_{light}(M=1) - I_{dark-surface}(M=1)} \quad (10)$$

4. Calculate the excess noise factor value at the applied reverse bias  $V$  by using the equations for  $\langle i_n \rangle$  (Equation 9) and  $M(V)$  (Equation 10).

The surface dark current is dependent on the bias. Each bias value shall be entered in the above equations separately and solved in the system of equations to find the best fit for the values of the  $F$ -factor at each bias.

#### f. Temperature Dependence of Avalanche Gain

Temperature dependence of APD gain is another critical parameter since any small change in the temperature can cause a dramatic change in the gain value in most applications.

Two factors influence the temperature dependence of gain: the semiconductor's bandgap shift with temperature and the breakdown voltage shift due to collisions of drifting carriers. For Silicon, the bandgap shift is more visible for wavelengths above 850 nm.

Figure 19 shows the quantum efficiency reduction as the temperature decreases for wavelengths above 850 nm due to a drop in the absorption coefficient value caused by the bandgap shift.

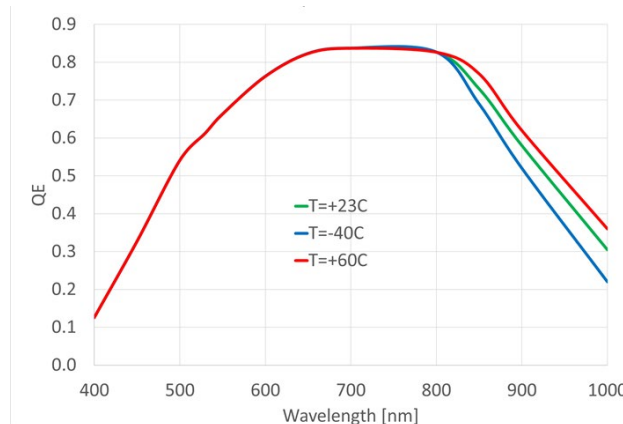


Figure 19. APD-800 QE with temperature for  $M=1$ .

With the rising temperature, drifting carriers have a higher probability of colliding with the host atoms of a semiconductor crystal, losing their energy to photons. This shifts the avalanche onset to higher voltages, increasing the breakdown voltage and reducing the gain at a given reverse bias.

Figure 20 is a typical example of a dramatic change in the avalanche gain with temperature for a front-illuminated Silicon APD with a buried multiplication layer.

Typical values for the breakdown voltage temperature coefficient for Silicon APDs are close to  $1\text{V}/^\circ\text{C}$ . The coefficient of the best commercially available APDs is slightly below  $\sim 0.7\text{ V}/^\circ\text{C}$ . If the avalanche gain stability is essential, the device temperature must be stabilized.

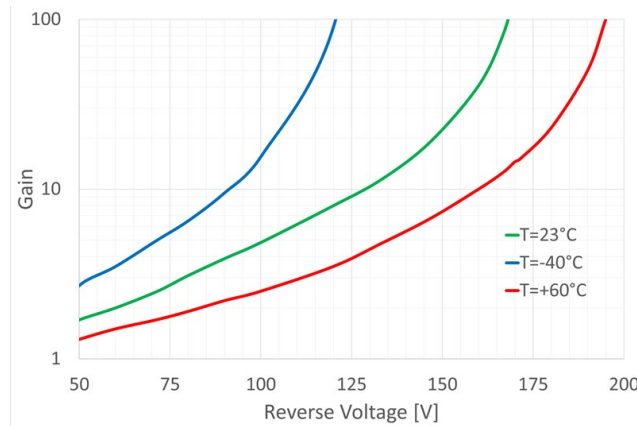


Figure 20. Example of the APD gain shift with temperature

## VII. Geiger-Mode APDs (SPAD)

Avalanche photodiodes operate in the analog (or linear) mode when the output current is proportional to the impinging light intensity. In another operating mode, incoming photons create an avalanche with gains of  $10^6$  or higher, allowing digital counting of incoming photons.

This type of APD operation is called the Geiger-mode or Single Photon Avalanche Detector (SPAD). Most APD structures can operate in the analog or Geiger mode of operation.

### a. Features of Geiger-Mode APD Structure and Operation

SPAD functions similarly to an analog APD, except the structure is optimized to sustain high internal amplification, allowing detection of the lowest light fluxes and low dark current enabling improvement of the detection efficiency.

An example of the APD structure for the Geiger-mode operation is shown in Figure 21. The structure features a very thin avalanche layer.

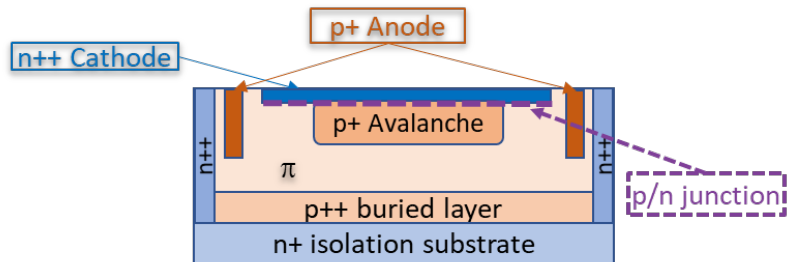


Figure 21. Schematic example of a Geiger-mode APD

The primary purpose of a Geiger-mode APD is to pass the operating point above the breakdown voltage, which allows the gains to exceed  $10^6$ . This is achieved only with structures with very low dark noise levels. The active area size can be minimized, and the operating temperature decreased close to zero degrees Celsius using thermoelectric coolers (TEC) to reduce the dark noise counts.

It is vital to apply an excess bias (overload voltage,  $A_{rm}$ ) if the device structure has a very low dark current (Figure 22). Although the excess bias is only a few volts in magnitude, it is enough to create an avalanche with more than a million ( $10^6$ ) gain on each incoming photon. As a result, the spike of the output current can reach a few pico-amps (pA) in amplitude, which the

downstream electronics can count. The device burns out if the avalanche is not quenched immediately after it reaches its maximum value. The quenching is discussed in more detail in the next section. Since the dark carriers also create an avalanche with the same amplitude as the output spike, the goal should be to minimize the dark count rate.

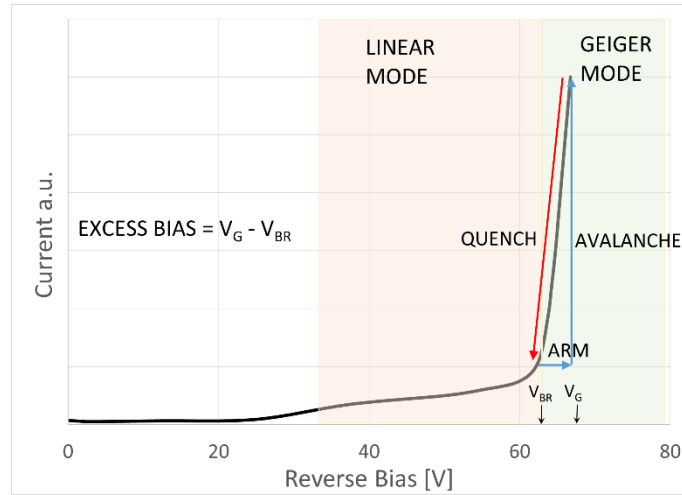


Figure 22. Schematic diagram showing operation of Geiger-mode APDs

The key performance parameters of Geiger-mode APDs are:

- Photon detection efficiency
- Dark count rate
- Timing resolution (*jitter*)
- After-pulsing probability (a false avalanche due to charge trapping-releasing, carrier tunneling, and intra-valley optical transitions)

Note that the excess noise does not apply to Geiger-mode APDs. Furthermore, the photon detection efficiency increases with the excess voltage. The fundamental SPAD trade-off is dark count rate and photon detection efficiency, which increases with bias.

## b. Geiger-Mode APDs (SPAD) Performance

Geiger-mode APDs operate when an effective avalanche quenching is established. The simplest way to quench the avalanche is to add a quenching resistor in series with the SPAD. In this scenario, after the avalanche starts, the resistance of the diode drops dramatically, and the current flow through the quenching resistor causes a voltage drop on the resistor, thereby decreasing the bias across the APD. This stops the avalanche.

Figure 23 is an example of a circuit providing passive quenching. The avalanche is quenched by discharging capacitance following an avalanche. The passive components of the quenching circuit can be assembled either inside the APD package or can be added as a part of an external circuit.

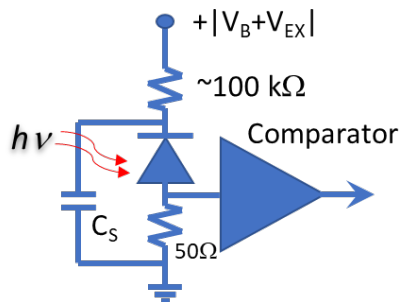


Figure 23. Example of an avalanche passive quenching

A critical drawback of passive quenching is the slow recharge of the capacitor  $C_s$ , which limits the dynamic range of the recorded optical signals.

Active quenching (see example in Figure 24) increases the avalanche quenching rate. It allows parasitics reduction, faster quenching, increased sampling rating, and afterpulsing reduction. Active quenching requires larger real estate for every single SPAD.

As an example, the achieved performance for a 50 mm diameter active area Silicon SPADs is:

- $V_{BR} < 30V$ ;  $PDE > 30\%-70\%$  for 400-800 nm
- $DCR < 10^4$  c/s @  $T = 23^\circ C$
- Time resolution  $< 1$  ns
- Timing jitter FWHM  $< 20$  ps
- Gain  $> 10^7$
- Excess bias (Arm overvoltage): 1.5 – 4V

Note that the performance for InGaAs SPADs is 10 times worse than that of Silicon SPADs.

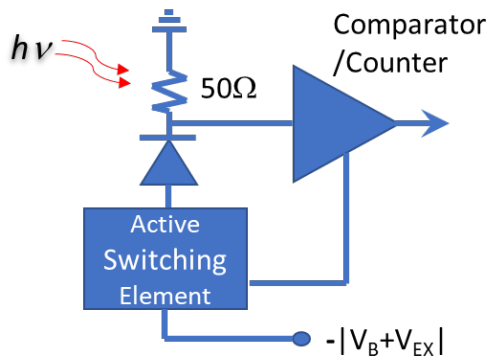


Figure 24. Example of avalanche active quenching

## VIII. Silicon Photomultipliers (SiPMs)

An array of Geiger-mode APDs can be designed with separate APD chips (dices); however, it requires large real estate consumed by the quenching control circuits. Placing an array of Geiger-mode APDs on a single chip also has its challenges due to the introduction of unwanted optical crosstalk between the elements. The crosstalk results from radiative transitions of avalanche electrons between sub-levels in the conduction band. The radiation can be observed under a microscope in a dark room. Biasing a Silicon APD at or slightly above the breakdown voltage (APD current must be limited) causes bursts of white light under a microscope. In the array of Geiger-mode APDs built on a single chip, a single burst within a cell of the array

triggers the avalanche in all surrounding cells, thereby blocking the entire array from detecting the signal of interest.

Silicon Photomultipliers (SiPM), or Micro-Pixel Photon Counter, can overcome the above issues.

### a. Silicon Photomultipliers (SiPMs) Structure and Performance Features

A Silicon Photomultiplier is a multi-pixel array of APDs operating in Geiger mode. The array consists of tens of thousands of pixels, with each pixel active area as small as 10 microns in diameter. SiPMs are not simple 2D arrays of Geiger-mode APDs. They are fabricated on a single Silicon chip, maximizing the fill factor for each array element. The quenching resistor for each microcell is manufactured on the same chip adjacent to the cell's active area, as shown in Figure 25.

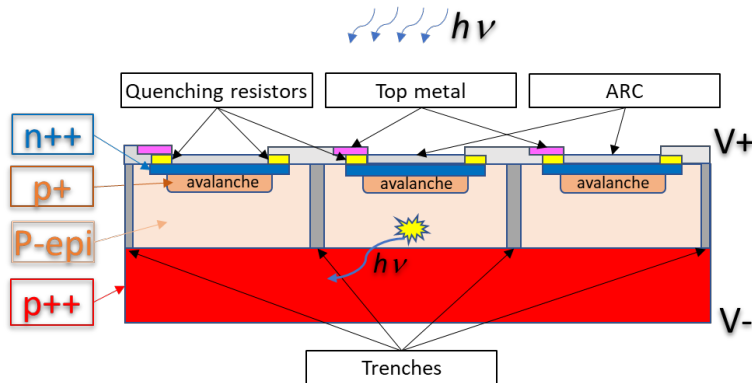


Figure 25. Example schematic structure of SiPM with trenches between active micro pixels

Trenches are fabricated between micropixels to eliminate the optical crosstalk. They block optical quanta generated due to intra-valley radiative transitions of avalanche electrons. Without these trenches, the optical crosstalk would fire the neighbor cells, preventing the operation of SiPMs.

The sources of noise in SiPMs are dark electrons avalanche, after-pulsing due to trapping/release of carriers in the avalanche region, electron tunneling effects, and optical crosstalk-initiated firing, which can be either eliminated entirely or significantly suppressed.

### b. Silicon Photomultipliers (SiPMs): Operation Basics

In a silicon photomultiplier, all microcells are connected in parallel. Each microcell includes the avalanche quenching resistor connected in series with the microcell. The output signal of a

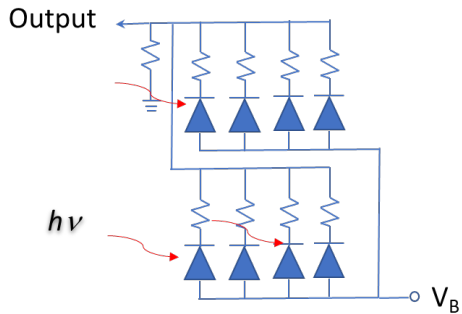


Figure 26. Electrical block-schematics of SiPM

SiPM is a sum of outputs from individual microcells (Figure 26).

When the array is illuminated with a uniform beam of light covering the entire array, consisting of only a single photon for a short period, the single photon can fire any microcell in the array with about the same probability.

Figure 27 exhibits the array's response to a single impinging photon when a single random microcell generates a brief spike of current with high amplitude.

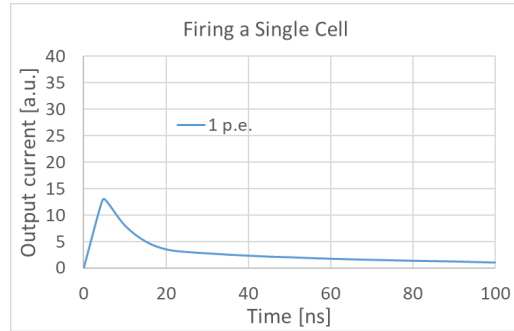


Figure 27. Photocurrent of SiPM in response to a single impinging photon

When two photons arrive simultaneously, then two microcells fire randomly, and the output current is two times larger in amplitude, as shown in Figure 28.

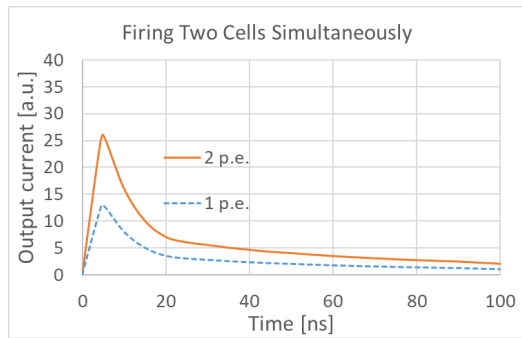


Figure 28. Photo-response of SiPM to two photons arriving simultaneously

Similarly, when three photons arrive simultaneously, three different microcells fire as a result, creating the output current three times larger than the signal from a single photon (Figure 29).

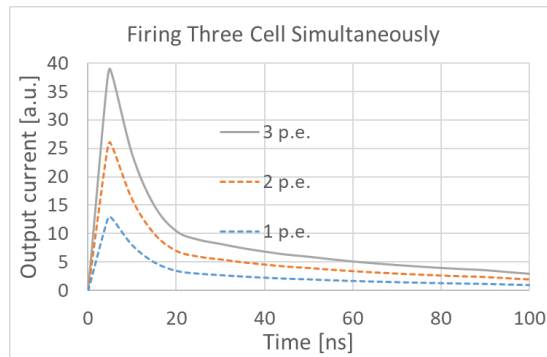


Figure 29. Photo- response of SiPM to three photons arriving simultaneously

The output current will have three time-spaced peaks when the incoming optical flux contains three photons arriving at different times (Figure 30).

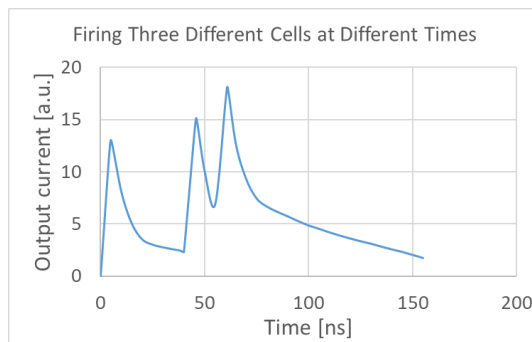


Figure 30. Photo- response of SiPM to three consecutive photons

### c. Silicon Photomultipliers (SiPMs): Output Signal

One can calculate the total number of optical quanta arriving at the detector by accumulating the total charge collected at the output of SiPMs during a short period.

The photoelectron spectrum of impinging light can be measured with a charge amplifier coupled to an analog-digital converter, showing well-resolved peaks, as shown in Figure 31.

The first peak is attributed to the firing of microcells by dark electrons (noise floor). The fourth peak with the highest amplitude indicates that most of the microcells were fired four times during the integration period, which means that three photons arriving at a time were the most probable event.

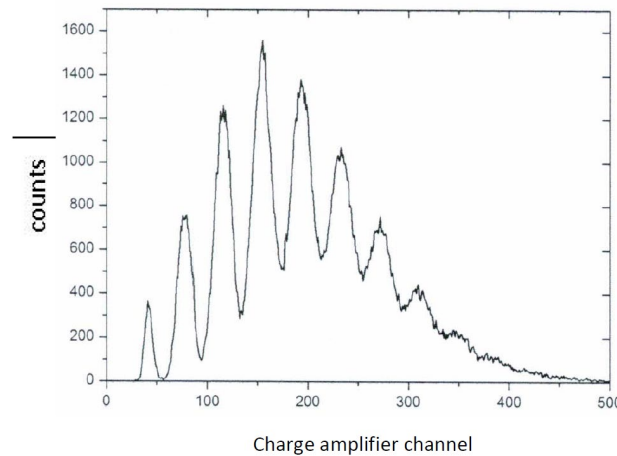


*Figure 31. Typical photoelectron spectrum recorded with SiPM coupled to charge amplifier*

The state-of-the-art SiPMs are manufactured with a 50 – 80% fill factor, meaning that more than half of a silicon chip is sensitive to light. The number of pixels per detector determines the dynamic range of a SiPM. The device saturates when the number of photons arriving at the same time approaches or exceeds the total number of micropixels.

The small value of Dark Count Rate of  $<10^5$  counts per second per  $1\text{ mm}^2$  allows detection of single photons during a brief period.

The pixel recovery time of  $\sim 20$  ns (for a SiPM with 25 mm micro-pixels pitch) is also noble, allowing secure detection of nanosecond-duration optical pulses.

## References

- [1]. R.J. McIntyre: Multiplication noise in uniform avalanche diodes, IEEE Trans. Electron. Dev. ED-13, 164–168 (1966).
- [2]. Joe C. Campbell, "Recent Advances in Avalanche Photodiodes," J. Lightwave Technol. 34, 278-285 (2016).